

# CO<sub>2</sub> capture on biomass-derived activated carbon: prolonged cyclic operation

Sonia Ben Yahia<sup>1\*</sup>, and Abdelmottaleb Ouederni<sup>1</sup>

<sup>1</sup>Chemical Engineering and industrial process Laboratory, Gabes engineering school, Gabes University, Gabes, 6029, Tunisia

**Abstract.** Cyclic carbon dioxide CO<sub>2</sub> adsorption-desorption experiments were conducted at ~295 K and a maximum pressure of 10 bar using laboratory-synthesized activated carbon pellets derived from almond shells. Over 20 cycles, the CO<sub>2</sub> adsorption equilibrium on these CA-Am-Pas pellets demonstrated stability from the 9th cycle onward, with adsorption efficiencies ranging from 1 to 0.8 and desorption yields around 40%. Equilibrium modelling across all cycles consistently showed the Freundlich isotherm as the best fit, achieving regression coefficients very close to 1.

## 1 Introduction

Rising atmospheric carbon dioxide CO<sub>2</sub> levels from fossil fuel combustion necessitate efficient capture technologies to mitigate climate change and meet net-zero goals. CO<sub>2</sub> capture via solid adsorbents offers a low-energy alternative to solvent processes plagued by corrosion and high costs. Biomass-derived activated carbons, especially from almond shells, excel due to high surface area (>1,500 m<sup>2</sup>/g), microporosity, and renewability.[1, 2, 3]

Key properties like narrow pore sizes (~0.4–0.7 nm) and surface chemistry drive capacity and cyclic stability. Precursors such as almond shells, date pits, and coconut husks yield superior CO<sub>2</sub> uptake (up to 5.5 mmol/g) via KOH/CO<sub>2</sub> activation. Recent 2025 studies highlight optimized date-palm AC and enhanced almond shell microporosity (32–36% gain).[1, 2, 4, 5, 6].

The present work is aimed to control the behaviour of a prolonged 20 adsorption – desorption cycles of CO<sub>2</sub> at 10 bars under low temperature on almond shell activated carbon pellets chemically activated (CA-Am-Pas). So that desorption yield, adsorption efficiency and cumulated amounts will be examine during this cyclic operation.

## 2 Materials and methods

### 2.1 Preparation of Activated Carbon Pellets

The manufacturing process of activated charcoal adopted in this study consists of three steps: firstly, the raw material is impregnated in a solution of phosphoric acid, then it is transformed

---

\* Corresponding author: [benyahya.sonia@gmail.com](mailto:benyahya.sonia@gmail.com)

into pellet form; subsequently, these pellets undergo a high-temperature heat treatment under a nitrogen atmosphere. In this section, we present the main characteristics of the precursor, the pre-treatment of the raw material, a description of the experimental process, and the various techniques used to determine the properties of the final product.

Throughout this study, almond shells precursors are used to produce activated charcoal in pellet form:

The almond shells, used as raw material for the production of activated charcoal, are harvested from almond trees in the Sfax region during the summer. They have a beige color and are in the form of small pieces of variable size, up to 3 to 4 cm.

**Table 1.** Manufacturing conditions of Almond shells

Raw materials	Almond shells
Nomination	CA-Am-Pas
Form	pellets
Manufacturing process	Chemical
Activation agent	H <sub>3</sub> PO <sub>4</sub>
step1 impregnation (Temperature, time & rate)	110 °C 9 h 1/3
Step2 carbonization (temperature & time)	410 °C 2h30min

## 2.2 Porosity and surface area

Textural analysis was performed by nitrogen adsorption/desorption at -196 °C over a relative pressure ranging from 9\*10<sup>-6</sup> to 0.99 P/P<sub>0</sub>. This characterization was carried out using an automated manometric apparatus

**Table 2 .** Textural properties

Activated carbon pellets	SpBET (m <sup>2</sup> /g)	Vpore (cc/g)	Vmicro(cc/g)	Vmésó(cc/g)	D pore (Å)	% vmicro	%vmésó
CA-Am-P	1184	0,5097	0,389	0,120	21,563	76,341	23,658

This table confirms that about three-quarters of the pore volume is microporous and one-quarter mesoporous,

So that, such a micro/mesoporous balance is advantageous: micropores give high capacity for small adsorbates, while mesopores (and the narrow peak near 2.5–3 nm) facilitate diffusion and access to the microporous network.

## 3 Experimental setup for volumetric technique

Throughout this work, a detailed analysis of the testing of vegetable-based pellets as adsorbents for carbon dioxide was conducted using a volumetric measurement setup (Figure 1) located at the Research Laboratory of Process Engineering and Industrial Systems (GPSI) at the National School of Engineers of Gabes [7]. This setup consists of two cylindrical cells:

Cell A: This is a stainless steel chamber, referred to as chamber VA and with a volume VA, connected to the feed bottle via valve V-1, serving as a volumetric reservoir to control the amount adsorbed.

Cell B: This is a measuring cell, with a volume VB, with a diameter of 6.3 cm and a height of 11 cm. inside this cell is a stainless steel mesh basket containing the activated carbon bed. The basket has a diameter of 5 cm and a height of 6 cm, and it is attached to a vertical axis that is rotated by an electric motor equipped with a speed reducer.

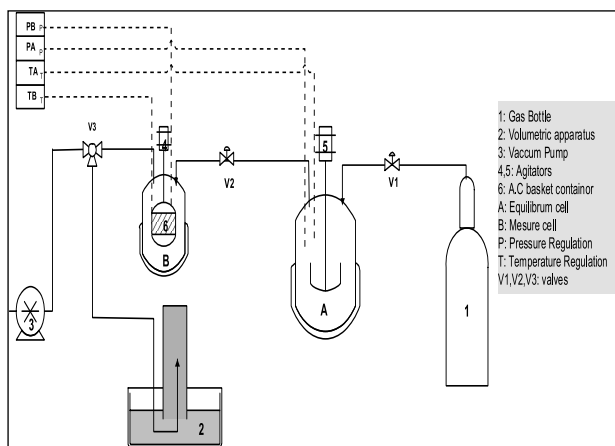


**Fig. 1.** Experimental setup

Carbon dioxide is stored on activated carbon pellets under specific operating conditions, which are summarized in the following table:

**Table 3.** Cyclic operation conditions

AC pellets	Cycle		Injections		P (bar)	m <sub>CA</sub> (g)
	Numbers	T (°C)	Numbers			
CACAm-Pas	20	22	6		10	20

Experimental Protocol and Method for Calculating Adsorbed/Desorbed Quantities:

Before adsorption step, the activated carbon amount has to be degassed under vacuum at high temperature during 2 hours. Adsorption step is consisted of 6 injections, each injection lead to an intermediate equilibrium state with an adsorbed amount  $n_{a,i}$ .

Desorption step is done after the finish of adsorption one by gradual depression the desorption amount of each depression is  $n_{d,i}$

In desorption curves,  $n_c$  is the cumulated amount and  $n_{rc,i}$  is the residual cumulated amount as shown in Figure 2.

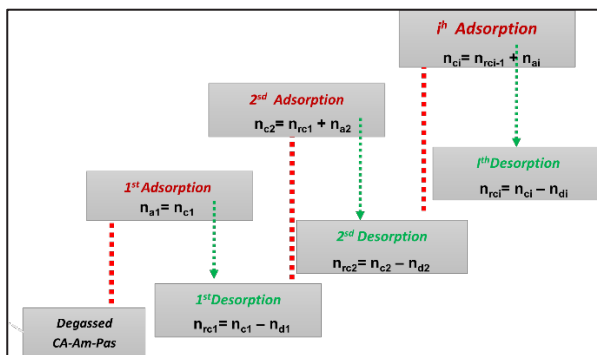


Fig. 2 : adsorption- desorption steps explication

## 4 Results and Discussion: Cyclic CO<sub>2</sub> capture on activated carbon pellets

### 4.1 CO<sub>2</sub> adsorption-desorption isotherms

In this section, CO<sub>2</sub> gas adsorption-desorption was performed at a maximum pressure of 10 bar at 22°C.

The curves for several adsorption-desorption cycles: cycle 1, cycle 5 and cycle 18 are grouped together in the following figure.

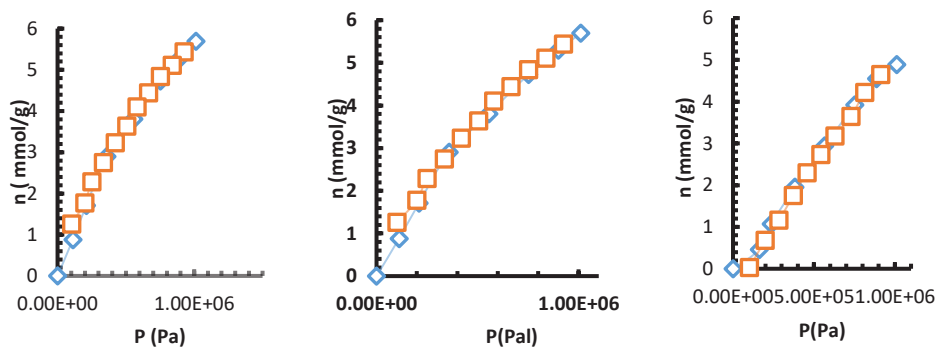


Fig. 3. Adsorption  $\diamond$  -desorption  $\square$  isotherms for the 1<sup>st</sup>, 5<sup>th</sup> and the 18<sup>th</sup> cycles under 22°C up to 10 bars

Examination of Figure 3 shows almost total reversibility for the different cycles, with a pattern similar to type I, which must be confirmed at a later stage by modeling the adsorption equilibrium throughout the cyclic operation.

As shown in previous curves (fig.3), it is clear that the phenomenon studied is quasi-reversible, with a very small difference between the two curves, confirming that physical adsorption is very different from chemisorption, with very low hysteresis. The steep initial slope at low pressure and continuous increase with pressure are typical of CO<sub>2</sub> adsorption on predominantly microporous activated carbons with additional mesopores. [8]

A maximum capacity near 5-5.5 mmol g<sup>-1</sup> at 22 °C and 1 MPa is consistent with high-surface-area, micropore-rich carbons and indicates that CA-Am-P is well suited for pressure-swing CO<sub>2</sub> capture or storage.

The nearly linear increase in loading at higher pressures implies that further capacity gains are possible at slightly higher pressures, while the relatively narrow hysteresis loop should facilitate regeneration during desorption cycle.

## 4.2 Evaluation of adsorption-desorption capacity during cyclic adsorption-desorption of carbon dioxide on activated carbon pellets based on almond shells CA-Am-Pas

### 4.2.1 Adsorption capacities

The adsorption capacity of an adsorbent defines the amount of gas that the material can adsorb under average pressure and temperature conditions. The most effective material is the one with the highest maximum adsorption capacity.

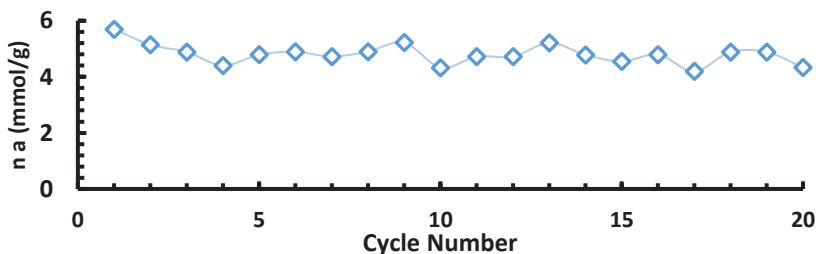


**Fig. 4:** CO<sub>2</sub> adsorption capacity on CA-Am-Pas undergoing cyclic testing.

High reproducibility was observed throughout the cyclic operation (fig4), with average adsorption around 4.8-5 mmol/g.

### 4.2.2 Efficiencies throughout the cyclic operation performed on activated carbon pellets made from almond shells

The adsorption efficiency of activated carbon is defined as the ratio of the quantity adsorbed in the  $i$ -<sup>th</sup> cycle to the quantity initially adsorbed by the virgin activated carbon in the first cycle.

$$e = \frac{n_{ai}}{n_{a1}} \quad (1)$$

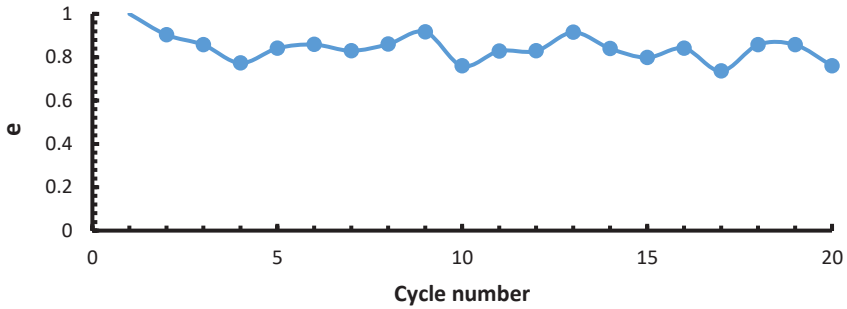


**Fig.5 :** Adsorption efficiencies throughout the cyclic adsorption-desorption process on activated carbon pellets made from almond shells.

Throughout the cyclic adsorption-desorption process, high efficiency is recorded, varying between 1 and 0.8, which proves the high quality of the activated carbon pellets and the almost total reversibility of the phenomenon.

#### 4.2.3 Desorption efficiency throughout the cyclic operation performed on activated carbon pellets made from almond shells

The desorption efficiency of the  $i^{th}$  cycle is defined as the ratio of the quantity desorbed in the  $i^{th}$  cycle to the sum of the quantity adsorbed in the  $i^{th}$  cycle  $n_{a,i}$  and the cumulative quantity from the previous cycle  $(i-1)$   $n_{rc,i-1}$

$$\alpha, i (\%) = \frac{n_{d,i}}{n_{a,i} + n_{rc,i-1}} * 100 \tag{2}$$

Where:

- $n_{a,i}$ : adsorbed amount per gram of Activated carbon (mmol/g) for the  $i^{th}$  cycle.
- $n_{d,i}$ : desorbed amount per gram of Activated carbon (mmol/g) for the  $i^{th}$  cycle.
- $n_{rc,i-1}$ : residual cumulated amount (mmol/g) for the  $i^{th}$  cycle as explained in Figure 2.

Figure 6 shows the desorption efficiency of activated carbon pellets throughout the 20 cycles studied:

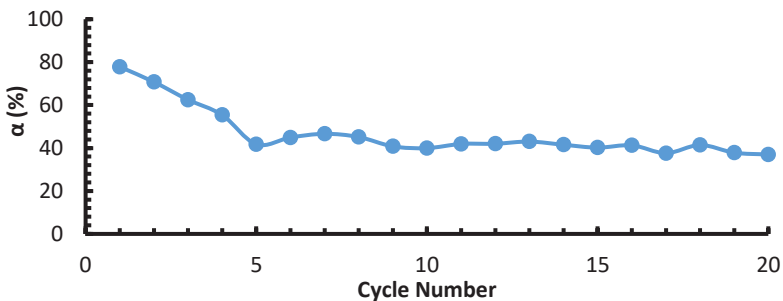


**Fig. 6.** Desorption yield throughout the cyclic adsorption-desorption process on activated carbon pellets made from almond shells.

This desorption efficiency reaches reproducible stability from the 9<sup>th</sup> cycle onwards, when the CA-Am-Pas pellets begin to exhibit stable and consistent behavior in desorbing the same amount of gas.

### 4.3 Modeling of CO<sub>2</sub> adsorption-desorption isotherms on CA-Am-P

In this section, three theoretical models Langmuir, BET and Freundlich of adsorption-desorption equilibrium were tested for the 20 adsorption isotherms obtained. Figure 7 summarizes the results of the regression factor R<sup>2</sup> obtained.

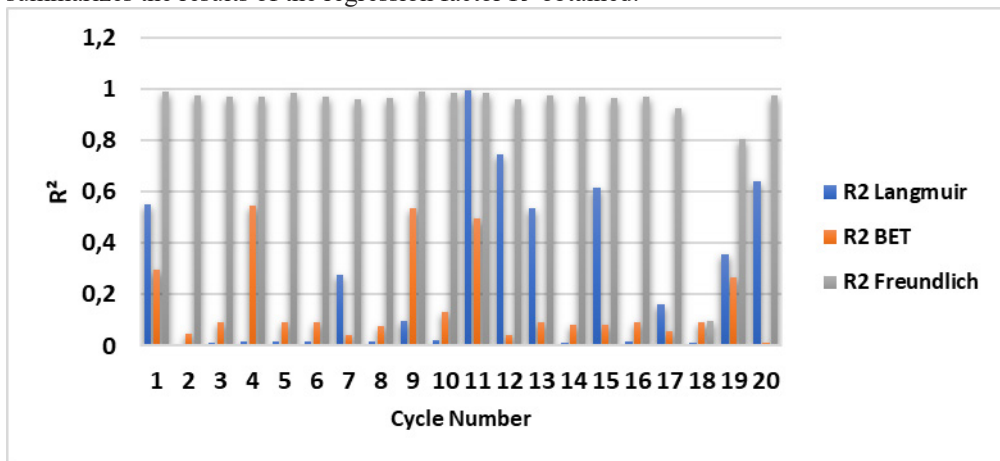


Fig. 7. Regression Factor for cyclic operation for the three models

Thus, the Freundlich model is the most appropriate model for these adsorption equilibria, confirming that these isotherms are type I and that there are no interactions between the adsorbed molecules and that each block of molecules is adsorbed at a single adsorption site. This model is adequate for all 20 cycles without exception and without modification at the beginning or end of this cyclic operation.[9]

## 5 Conclusion

This work has brought together a whole series of successive experiments on the same sample of activated carbon pellets made from almond shells under a maximum pressure of 10 bar relative and at T = 22°C.

This operation showed stability from the 9th cycle onwards, where the cumulative quantity and desorption stabilized at an efficiency of  $\alpha = 40\%$ , an adsorption capacity of around 5 mmol/g, and a desorption capacity of around 4.2 mmol/g.

Modeling of the adsorption equilibrium confirmed the suitability of the Freundlich model from the 1<sup>st</sup> to the 20<sup>th</sup> cycle, confirming type I isotherms and the physisorption of CO<sub>2</sub> molecules in CA-Am-Pas pellets.

## References

1. M. M. Bade, A. A. Dubale, D. F. Bebizuh, and M. Atlabachew, “Highly Efficient Multisubstrate Agricultural Waste-Derived Activated Carbon for Enhanced CO<sub>2</sub> Capture,” ACS Omega, vol. **7**, no. 22, pp. 18770–18779, Jun. 2022, doi: 10.1021/acsomega.2c01528.
2. S. M. Bouzgarrou et al., “Analysis of the CO<sub>2</sub> adsorption on AC: experimentation and statistical studies,” Sci. Rep., vol. **15**, no. 1, Dec. 2025, doi: 10.1038/s41598-025-22526-w.

3. H. Boulika, M. El Hajam, M. Hajji Nabih, N. Idrissi Kandri, and A. Zerouale, “Activated carbon from almond shells using an eco-compatible method: screening, optimization, characterization, and adsorption performance testing,” *RSC Adv.*, vol. **12**, no. 53, pp. 34393–34403, Nov. 2022, doi: 10.1039/d2ra06220h.
4. E. H. Al-Ghurabi, M. M. Boumaza, W. Al-Masry, and M. Asif, “Optimizing the synthesis of nanoporous activated carbon from date-palm waste for enhanced CO<sub>2</sub> capture,” *Sci. Rep.*, vol. **15**, no. 1, Dec. 2025, doi: 10.1038/s41598-025-00498-1.
5. K. Nikolić et al., “Sustainable Carbon Source from Almond Shell Waste: Synthesis, Characterization, and Electrochemical Properties,” *Materials*, vol. **19**, no. 1, Jan. 2026, doi: 10.3390/ma19010008.
6. N. Noorani, S. Pourebrahimi, and A. Mehrdad, “Enhancing CO<sub>2</sub> adsorption performance of cold oxygen plasma-treated almond shell-derived activated carbons through ionic liquid incorporation,” *Journal of CO<sub>2</sub> Utilization*, vol. **88**, Oct. 2024, doi: 10.1016/j.jcou.2024.102927.
7. S. Ben Yahia., “Stockage du méthane par adsorption sous pression sur du charbon actif microporeux à base de grignons d’olives.”, Ph.D. dissertation, 2013.
8. S. M. Bouzgarrou, H. Jedli, R. Hassani, E. Sabi, A. H. Khan, and K. Slimi, “Investigation of the CO<sub>2</sub> adsorption isotherms on activated carbon by statistical physics treatment,” *Sci. Rep.*, vol. **15**, no. 1, Dec. 2025, doi: 10.1038/s41598-025-16088-0.
9. D. M. Glenna et al., “Carbon Capture: Theoretical Guidelines for Activated Carbon-Based CO<sub>2</sub> Adsorption Material Evaluation,” *Journal of Physical Chemistry Letters*, vol. **14**, no. 47, pp. 10693–10699, Nov. 2023, doi: 10.1021/ACS.JPCLETT.3C02711.